Journal of Magnetic Resonance 259 (2015) 216–224

Contents lists available at ScienceDirect

Journal of Magnetic Resonance

journal homepage: www.elsevier.com/locate/jmr

Air core notch-coil magnet with variable geometry for fast-field-cycling NMR

S. Kruber, G.D. Farrher, E. Anoardo *

Laboratorio de Relaxometría y Técnicas Especiales, Grupo de Resonancia Magnética Nuclear, Facultad de Matemática, Astronomía y Física, Universidad Nacional de Córdoba and IFEG – CONICET, Córdoba, Argentina

ARTICLE INFO

Article history:
Received 27 June 2015
Revised 24 August 2015
Available online 5 September 2015

Keywords:
Fast-field-cycling
Magnet system
Optimization
Notch-coil

ABSTRACT

In this manuscript we present details on the optimization, construction and performance of a wide-bore (71 mm) α-helical-cut notch-coil magnet with variable geometry for fast-field-cycling NMR. In addition to the usual requirements for this kind of magnets (high field-to-power ratio, good magnetic field homogeneity, low inductance and resistance values) a tunable homogeneity and a more uniform heat dissipation along the magnet body are considered. The presented magnet consists of only one machined metallic cylinder combined with two external movable pieces. The optimal configuration is calculated through an evaluation of the magnetic flux density within the entire volume of interest. The magnet has a field-to-current constant of 0.728 mT/A, allowing to switch from zero to 0.125 T in less than 3 ms without energy storage assistance. For a cylindrical sample volume of 35 cm^3 the effective magnet homogeneity is lower than 130 ppm.

1. Introduction

Fast-field-cycling (FFC) nuclear magnetic resonance (NMR) is a well-established experimental method for determining certain physical properties in a wide-range of materials [1–5]. The method is particularly useful to perform NMR experiments at low magnetic fields, where conventional methods exhibit severe limitations due to the signal-to-noise (S/N) ratio degradation of the free induction decay (FID) or NMR signal. While the magnetic field is cycled between different values according to the selected experiment, the signal detection field is fixed. In consequence, the probe as well as the receiver electronics are usually optimized for a fixed working frequency, which is independent of the Larmor frequency at which the nuclear spin system evolves.

A critical part of any electronic field-cycling apparatus is the electromagnet. It defines the general performance of the instrument, in close dependence with the electric power management and control electronics. Desired features for this sort of machines are: (i) The achievement of high magnetic flux densities, thus favouring the S/N ratio of the FID while increasing the dynamic range of the instrument. (ii) A fast switching of the magnetic flux density, thus allowing the observation of nuclear magnetic events associated with short relaxation times and eventually, the access to zero-field NMR spectroscopy. (iii) The spatial field homogeneity of the magnetic flux density within the sample volume should be conveniently compatible with, at least, low-resolution NMR. It is then possible to summarize the three main requirements for a FFC electromagnet:

- The generation of a maximal possible magnetic flux density for a given power ($B_{max}(P)$).
- The switching between the different magnetic flux densities performed in minimal time (dB/dt).
- The achievement of an adequate homogeneity inside a given volume of interest, where the sample will be located ($\Delta B/B$).

Due to the mutual interrelation between these requirements, the optimization process is a challenging task. Different air-core electromagnet designs can be found in the literature [6–8]. Schweikert's [7] and Lip's [8] magnets are based on non-uniform current-carrying paths performed on metallic cylinders. Concentric cylinders are assembled together in order to reach the desired magnetic flux density. This approach allowed to produce magnets with excellent electric performance for the fast switching (a few ms) of magnetic fields over 1 T. In both cases, the machining process requires the cutting of complicated helix profiles along the metallic cylinders. As a consequence of the non-uniform current distribution, the power dissipation along the coil is localized.

In a recent paper we described the optimization method for variable notch-coil magnets that, in addition to the typical

* Corresponding author.
E-mail address: anoardo@famaf.unc.edu.ar (E. Anoardo).

http://dx.doi.org/10.1016/j.jmr.2015.08.015
1090-7807/

requirements, have a tunable homogeneity within the sample volume and an uniform heat dissipation along the magnet body [9]. A novel calculation procedure was introduced by considering a more realistic model of the magnet with broken azimuthal symmetry. The design was compared with other existing geometries [7,8], arriving to the conclusion that the concept of a notch-coil magnet with variable geometry is suitable for its application in FFC-NMR. It provides a reasonably good field-to-power ratio, while having the advantage of an uniform heat distribution along the cylinders, an adjustable field homogeneity and a much simpler machining process. In this work we present details of a prototype notch-coil magnet with variable geometry (hereinafter the notch-coil). To test the concept, a wide-bore version was considered for large sample sizes (25–35 cm^3) with a bore diameter of 71 mm.

The material choice for the magnet manufacture is not a minor point: the resistivity has a direct impact on the coil resistance, and then, on the thermal stress along the magnet and the switching performance [1,3]. Since the present set-up is mainly intended for an evaluation of the calculated geometry, that is, the capacity to get an adjustable homogeneity and the calculated field-to-power ratio (according to the material choice), the prototype was made in aluminium. Although much costly, a silver version would have a much lower resistance. Copper represents an intermediate option but, its mechanization may turn tricky compared to aluminium.

An uniformly distributed power dissipation along the magnet body results attractive when pushing the system to extreme operation. In contrast to variable-pitch solutions, local heating is absent in the notch-coil design. As a consequence, thermal dilatations are also uniformly distributed. The variable geometry may be used to compensate magnetic field shifts and homogeneity looses due to the thermo-mechanical stress of the magnet at high conductive regimes. It is worth to mention that up to now, only drifts of the magnetic flux density due to thermal effects have been electronically compensated [2]. Although not yet implemented, the system may turn auto-adaptive with a proper control feedback. It can also be used to partially compensate weak magnetic field gradients originated at external sources, or even to produce pulsed fields with a given inhomogeneity (the magnet may switch between homogeneous and non-homogeneous configurations during the cycle of the experiment).

2. The notch-coil prototype

The electromagnet has to satisfy a reasonable compromise between the three basic requirements mentioned in the previous section: a maximal magnetic flux density for a given power, a minimal switching time and an acceptable field homogeneity. We impose the additional demands of an adjustable field homogeneity and a uniform power distribution along the magnet body. All these conditions can be fulfilled by a notch-coil geometry [9]. In general, a notch-coil magnet consists of metal cylinders with a helical cut as the base for the current-carrying path. It is composed of a given number of inner layers, which generate the main magnetic flux density. In addition, notch layers contribute with the correcting magnetic flux density that homogenizes the field distribution inside the volume of interest. The layers are coaxially assembled with a minimum radial gap between them to increase the maximum flux density for a given current (but correctly dimensioned to facilitate an efficient cooling). Various configurations of notch-coil magnets are possible [10,11]. However, outer notch-coils facilitates the design in view of the desired higher magnetic flux density with adjustable homogeneity. The field homogeneity can be modified by varying the position of the outer notch layers. Both the linear movement along the longitudinal axis and the rotation about it should be considered. However, the assembly considering both degrees of freedom turns complicated (see Section 3).

The magnet prototype here presented corresponds to a large coil having a wide-bore. Compared to a smaller magnet intended for standard 10 mm in-diameter samples, both the resistance and the inductance are higher, while the magnetic flux is lower for an equivalent electric power. The considered prototype was consequently calculated with a single inner layer in order to limit the total resistance and inductance of the magnet (see Fig. 1). This choice also limits the maximum field. The used configuration allows to capture proton NMR signals at about 5 MHz, which is by far reasonable for the present purpose.

The necessary parameters to describe the notch-coil geometry are indicated in the half sectional view of Fig. 2. These are:

- The inner $r_{i/inner}$ and outer $r_{o/inner}$ radii of the inner-coil cylinder.
- The half length l_{inner} of the helix corresponding to the inner-coil cylinder.
- The radii $r_{i/notch}$ and $r_{o/notch}$ of the notch layers.
- The length l_{notch} of the notch-coil helix.
- The distance $l_{position}$ between the outer edges of the helices of the notch and the inner layer at each side of the magnet.
- The gap g between the coaxial cylinders.

Other important parameters are the pitch (p) of the helices, the cut width (c) and the number of turns of each layer (N_{inner}, N_{notch}). The mathematical methodology used to calculate the prototype has already been described in an earlier publication [9]. For completeness, a brief survey is included in the Appendix.

During the optimization process, the parameter N_{notch} was varied in steps of one turn and d (see Appendix) in steps of 125 μm, in concordance with our machining and positioning tolerances (see Section 3). The *percentage volume coverage* ($PVC_{homogeneity}$) was calculated for a field homogeneity of 10 ppm (this parameter $\times 100$ measures the percentage of calculated points for the magnetic field map within the volume of interest, having equal or less homogeneity to a given value, see the Appendix). The magnetic flux densities were always calculated in $11^3 = 1331$ k-nodes of a cubic mesh with a lateral length of $a = 70$ mm, and by changing the parameter N_{inner} between the values $80 < N_{inner} < 120$ in steps of $\Delta N_{inner} = 2$. The highest achievable PVC_{10ppm} values for each N_{inner} are displayed in Fig. 3. The figure also shows the maximal magnetic flux density for a power of 10 kW ($B_{max}(10\,kW)$) for each optimal configuration. The plot allows to speculate on how the three main requirements are simultaneously satisfied by each configuration. It is highly desirable to have both PVC_{10ppm} and $B_{max}(10\,kW)$ as high as possible, with the minimum possible number of turns (in order to limit the inductance ($\sim N^2$) and resistance ($\sim N$) of the coil-system). The rectangle

Fig. 1. Schematic view of the magnet system.

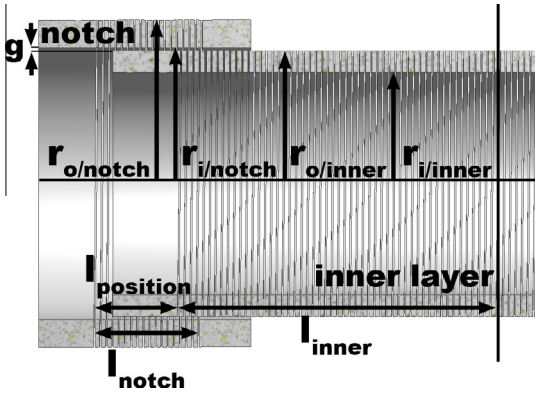

Fig. 2. Half section view of the magnet system design with the corresponding parameters. Only the left hand side of the magnet system is shown.

indicates the chosen configuration ($N_{inner} = 104$) for the technical realization. The resistance of each cylinder was estimated from:

$$R \approx \rho \frac{\sqrt{r_{mean}^2 + p^2}(\varphi_2 - \varphi_1)}{(2\pi p - c)(r_o - r_i)} \quad (1)$$

where ρ is the electric resistivity and φ_1, φ_2 are defined in the Appendix. An aluminium alloy with $\rho \approx 5.2 \cdot 10^{-8}\ \Omega\,\mathrm{m}$ was used.

Initial calculations were carried out by approximating the current-carrying paths by infinite small wires. To reach a better approximation, it has proved sufficient to consider a superposition of $m \times m$ current filaments [12,13]. After the optimal set of parameters is found (number of turns and position of the notch elements), the field distribution of the magnetic flux density is recalculated for a more realistic conductor geometry, by approximating the current distribution as a superposition of current filaments which are uniformly distributed along the conductors. Then a correction in the positions of the outer notch pieces is obtained. Values shown in Fig. 3 are all obtained by this procedure. The calculation is made in two steps: a first calculation using a coarse-grained mesh having only 300 k-nodes allow to get an approximated solution in a few hours (using an Intel 4-cores $i7$ processor at 3.07 GHz). Then, a second run is performed by scanning for the optimal solution within a closer interval around the previously calculated configuration. This time the field is calculated at the 1331 k-nodes (about 46 h).

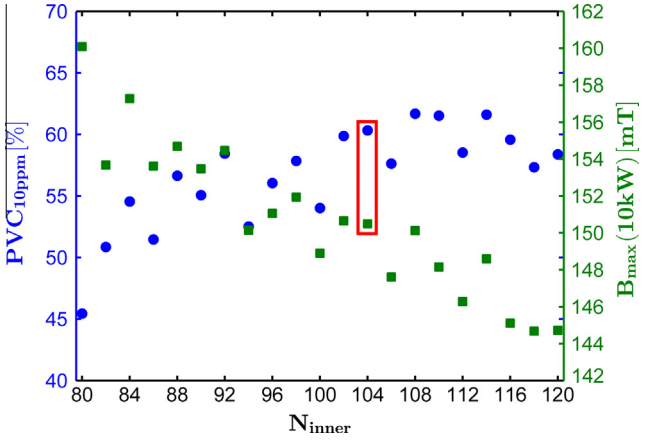

Fig. 3. PVC (circles) and maximal magnetic flux density (squares) for the various configurations of the prototype. The power is set to $P = 10$ kW. The rectangle indicates the selected configuration ($N_{inner} = 104$).

Table 1
Parameters of the single layer notch-coil.

$r_{i/inner}$	35.50 mm
$r_{o/inner}$	42.50 mm
$r_{i/notch}$	43.50 mm
$r_{o/notch}$	52.20 mm
l_{notch}	35.17 mm
$l_{position}$	72.92 mm
c	0.50 mm
l_{inner}	101.61 mm
g	1.00 mm
p	1.95 mm/2π
N_{inner}	104
N_{notch}	18

A single inner layer magnet having $N_{inner} = 104$ turns was considered for the prototype. The remaining geometric parameters are depicted in Table 1.

The calculated homogeneity is shown as contour plots for the xz and yz planes, as well as for the z-axis in Fig. 4. The theoretical electric characteristics of the prototype are summarized in Table 2. The inductance was approximated by considering circular conductors with rectangular cross section [14–16].

3. Machining and assembly of the magnet system

The main task in machining and assembling the magnet is to reach a final performance consistent with the theoretical design. Any deviation from the calculated magnet would lead to homogeneity degradations. It was verified from the calculations that an uncertainty in the cut width up to ±0.2 mm only affects the homogeneity in less than 1 ppm. On the contrary, a difference of 0.2 mm in the cylinders diameters may affect the homogeneity up to 20 ppm. These numbers were obtained by introducing deviations in the mentioned dimensional quantities and evaluating the changes in the magnetic field map. With this picture in mind, a special set-up was implemented for the mechanization of the magnet.

Fixed pitch helices were cut into aluminium cylinders using a special set-up based on an Eila ARMEX lathe (Córdoba – Argentina). A special cutting tool was designed using a Siemens 2CW5187-2 electric motor (Germany). A HSS (High Speed Steel) circular saw from Sin Par (Quilmes – Argentina), thickness 0.5 mm, was used as a cutting element. The attack-angle of the saw was set with a precision of 0.1 degrees. A continuous cut was performed by controlling the linear and angular velocity of the lathe chuck which holds the aluminium cylinder. The lathe provided a feed of 1.95 mm per rotation, in concordance with the calculated pitch. The precision in the linear position of the saw was 0.1 mm. The needed depth in the cut was achieved after a repetition of the cutting cycle 36 times for the internal cylinder and 45 times for the notch elements. Fig. 5 shows a machined notch element.

According to the optimization a clockwise cut was machined for the inner layer, while anticlockwise for the notch layers (this serves to compensate axial inhomogeneity due to the helical structure). This feature is also necessary for the electrical connections in the final assembly.

The cuts were sealed with an epoxy glue (Poxypol) to assure a better mechanical stability and to facilitate the flow of the coolant between the layers. The high viscous glue was pressed inside the helical cuts using a specially designed assembling at a pressure of 48.5 kPa, provided by a 10 t hydraulic press (CINAR, Rosario – Argentina). The cylinders lengths and their final outer and inner radii were finalized by lathing them again with a precision of 0.05 mm.

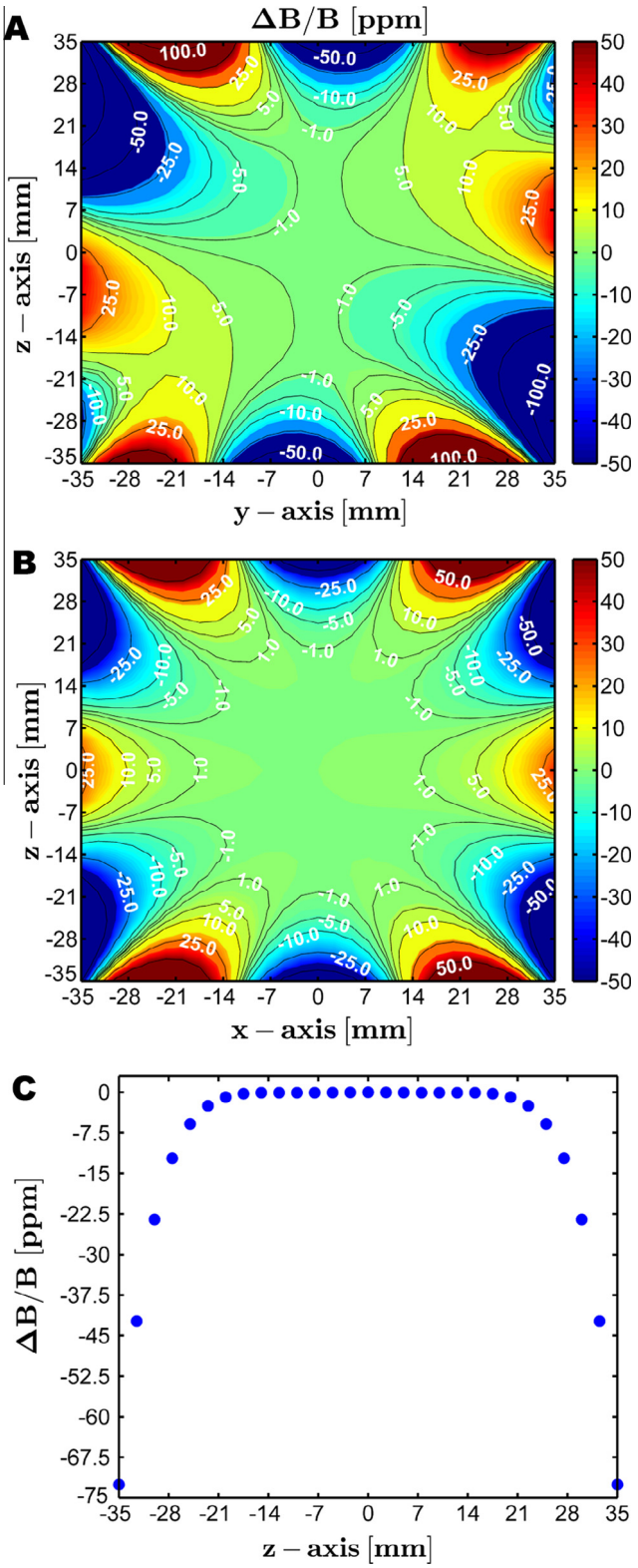

Fig. 4. Contour plots of the theoretical field inhomogeneities for (A) the *yz*-plane, (B) the *xz*-plane and (C) for the *z*-axis of the prototype.

The assembly of the system satisfies both an efficient cooling and the mobility of the notch elements according to the variable geometry considerations of the design. Fig. 6 shows a schematic half sectional view of the final assembly of the prototype. All parts are encapsulated inside a glass cylinder which is closed by two plates of polycarbonate located at each side of it. These plates have the entrances/exits for the coolant (DEX-Cool), electric connections and threaded rods to move the notch-holders. Special notch-coil holders encapsulate the corresponding notch-coil. Two threaded bars for each notch-coil holder are used to position them along the axial direction of the magnet system. The notch-coil holders are designed so that the cooling liquid can flow inside and outside of the notch-coils. Between the notch-coil holders, another hollow cylinder is placed in the middle to ensure the flow of the cooling liquid between the outside of the inner layer and inside of the notch-coils. The threaded bars are connected to turning knobs to facilitate the positioning of the notch-coils. The pitch of the thread has 1 mm per turn and the turning knobs can be positioned in 24 steps per rotation, providing a step size for the notch-coils in axial direction of approximately 40 μm. Each notch can be positioned independently, by turning the corresponding pair of knobs at the same rate. The assembly is designed to have the coolant flow in contact with both sides of the layers, across the axial direction of the magnet system (see Fig. 6). Two O-rings are placed between the external face of each notch-holder and the inner wall of the glass tube, so that the coolant always flows through its designated paths (with a flow-rate of 12 m^3/h). The electrical connections were made out of copper. The layers were connected to flexible copper sheets supporting the movements of the notch-coils. Fig. 7 shows the final assembled prototype.

Table 2
Calculated characteristics for the prototype magnet system. The table also includes the calculated magnet current I for a supply voltage of $U = 41.8$ V.

B_{max}(10 kW)	150.5 mT
R	175.0 mΩ
L	192.6 μH
$V_{interest}$	35 cm^3
PVC_{10ppm}	60.3%
I	239 A
U	41.8 V

4. Test and characterization of the magnet prototype

The resistance and inductance of the coil were measured using an electronic LCR meter INSTEK model LCR-819 GW (Taipei – Taiwan): $R = (181.4 \pm 0.2)$ mΩ and $L = (177 \pm 1)$ μH. A modified Spinmaster field-cycling relaxometer from Stelar (Mede – Italy) was used to perform the NMR testing of the magnet.

Fig. 8 illustrates the linear behavior between the current across the magnet and the generated magnetic flux density. The magnetic flux density was measured using a Lake Shore 475 DSP hall meter (Westerville, OH, USA) equipped with a HMNA-1904-VR hall-probe during a 4 s field-pulse. The current was obtained from the

Fig. 5. Finalized machined notch element.

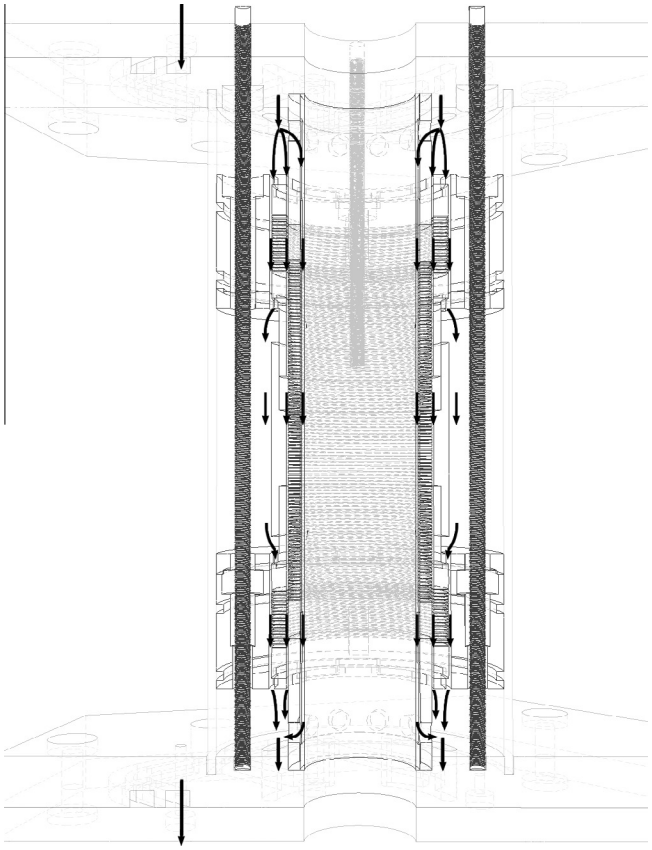

Fig. 6. Half section of the magnet assembly. The arrows indicate the flow of the coolant in axial direction.

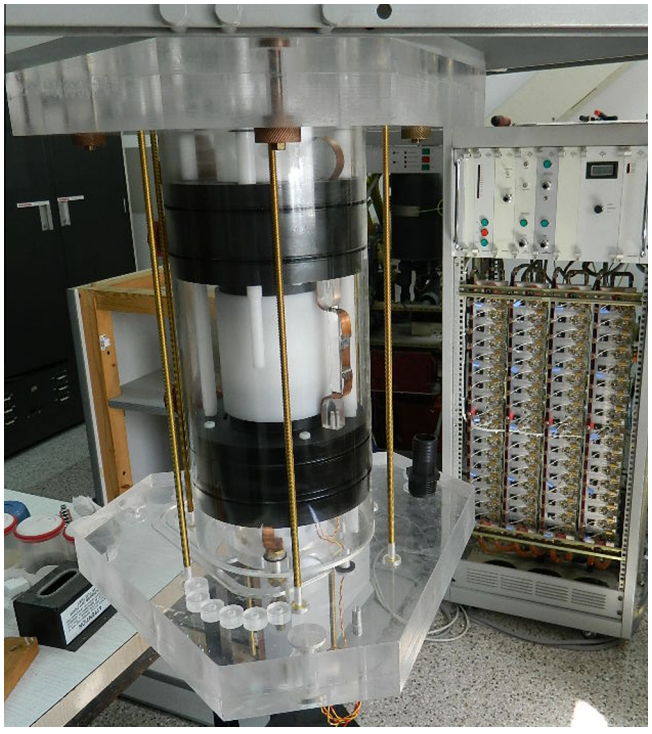

Fig. 7. Assembled prototype. Behind, transistor bank and control unit of the modified Stelar instrument used to test the prototype.

voltage-drop, measured using an Agilent U1252A multimeter (Santa Clara, CA, USA), in a series resistor of (7.8 ± 0.2) mΩ. A

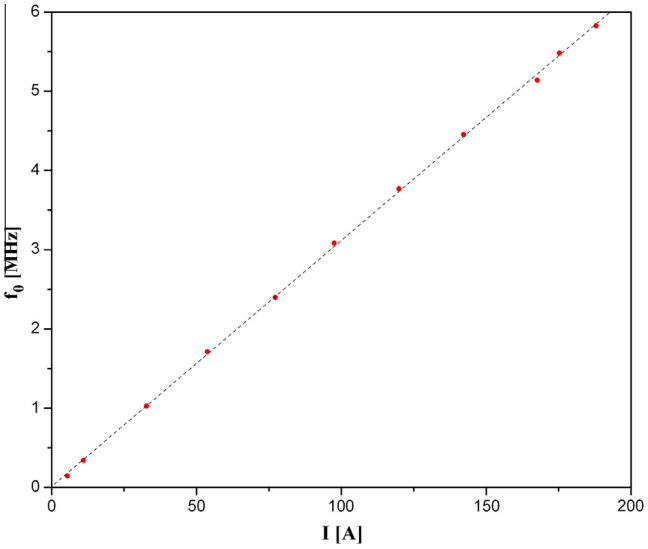

Fig. 8. Linear relationship between the magnet current and the magnetic field as measured through the NMR signal frequency. Data point sizes represent experimental errors. The dashed line is added to guide the eye.

field-to-current constant $K = B/I = 0.728$ mT/A was obtained from the plot shown in Fig. 8.

A silicon temperature sensor KT 110/TO-92 Mini (Infineon Technologies, Germany) was permanently located at the center of the external face of one notch layer. According to approximated calculations and preliminary experimental tests (before assembling the magnet into the cooling chamber), the temperature of the inner cylinder is expected to be higher than the temperature of the notch (about 30% in the absence of cooling, although this difference may be lower under cooling conditions). The sensor was installed in the notch to simplify the connexion, with the assumption that temperature of the inner layer would never be higher that 30% of the measured value. Fig. 9 shows the thermal response after current pulses of different length and intensity. The corresponding thermal drifts of the magnetic field were recorded in terms of the relative frequency shifts of the FID signal following a 2 s field-pulse (see Fig. 10). No electronic compensation was used.

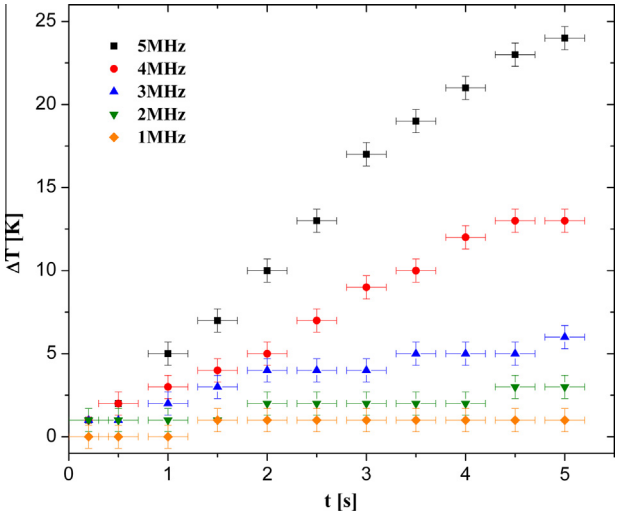

Fig. 9. Thermal response of the magnet after current pulses with variable length and intensity. All thermal jumps start from an initial magnet temperature of 300 K.

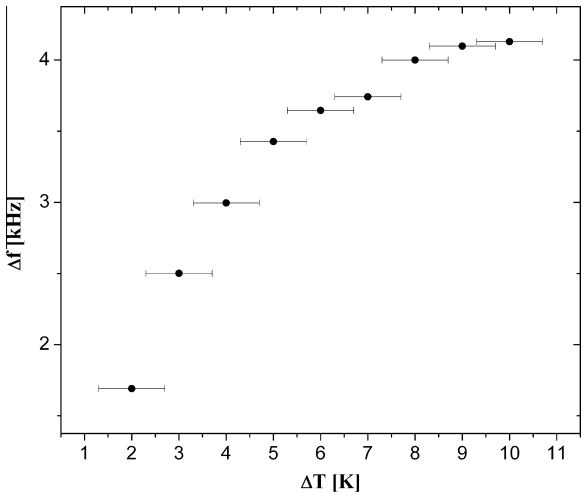

Fig. 10. Relative frequency shift of the FID signal as a function of the relative temperature change of the magnet.

^{1}H NMR signals were acquired under different magnet conditions at a fixed detection frequency $f_{det} = 5$ MHz, using a non-polarized magnetic field sequence [2] with a relaxation field of $f_{rel} = 4.975$ MHz. A sample of water slightly doped with copper sulfate, $T_1 \approx 20$ ms, was used. FID signals were acquired using a fully home-made probe-head based on a saddle coil (6.5 μH). All the elements including the RF coil itself as the tuning and matching variable capacitors (50–100 pF) were designed and implemented in the laboratory. The probe (parallel tank with a series matching capacitor) was pre-tuned using an Agilent 8712ET Network Analyzer, and tuned once in the magnet with the sample located within the RF coil volume using the tuning facility available from the Stelar instrument console. The probe can be tuned from 4.4 MHz to 6.3 MHz. All experiments were carried out at room temperature.

Fig. 11A and B shows the recorded NMR signals for different sample volumes at a fixed position of the notch-elements. In both cases the sample was centred inside the radio-frequency (RF) coil. The sample container has an inner diameter $d_i = 26.5$ mm and an approximate height of $h \approx 63.5$ mm resulting in a total volume of $V \approx 35$ cm^3. This sample container fits the available volume inside the RF coil. Fig. 11A corresponds to a sample volume of 25 cm^3 ($h \approx 45.3$ mm) while Fig. 11B to 35 cm^3. The best FID was otained with ($V \approx 25$ cm^3), in consistence with the calculated magnetic field map, see Fig. 4. This corresponds to the optimal position of the notch elements.

Fig. 12 shows the dependence of the FID signal with the position of the notch layers. Starting from the optimal position, the notch layers were moved inwards and upwards, that is, both notch elements become closer ($d < d_{opt}$) or, they depart from each other ($d > d_{opt}$). The graph represents the calculated line widths and signal intensity. The signal deteriorates when the notch layers are departed from the optimal position, regardless in which direction they are moved. However, the FID can still be easily observed within a range of $d = d_{opt} \pm 3.15$ mm.

An important feature of a variable geometry magnet is the possibility to compensate for the homogeneity of the magnetic flux density inside the volume of interest at any time. This bears the advantage to partially recover the field homogeneity which might be degraded by any distortion of the magnet itself (for example, geometry changes due to thermo-mechanical stress), or due to the presence of an additional field originated at external sources, etc. To test this possibility, an external magnetic flux density was

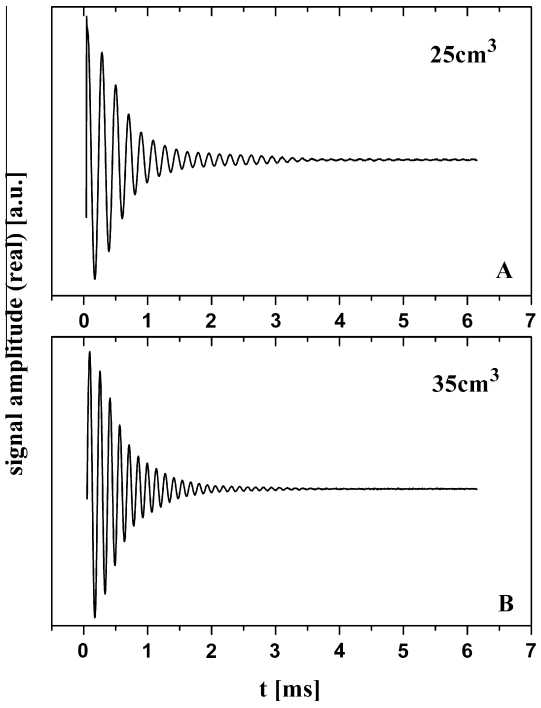

Fig. 11. Captured ^{1}H NMR signals for different sample volumes. (A) $V \approx 25$ cm^3. (B) $V \approx 35$ cm^3.

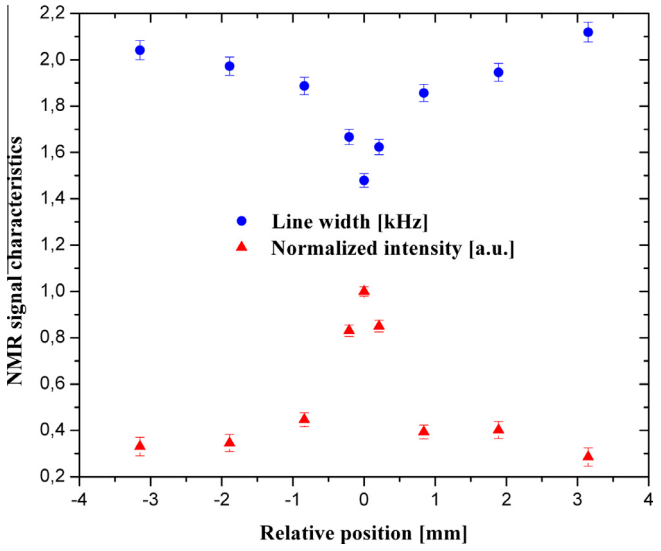

Fig. 12. Line widths and intensities of the ^{1}H NMR signals for a volume of $V \approx 25$ cm^3 as a function of the position of the notch layers. In this graph, zero represents the optimal position. Positive values of the relative position represent the situation where the distance between the notch coils is increased. The contrary holds for negative values. Signal intensities are normalized to the amplitude of the FID corresponding to the optimal position. The concept of "tunable" magnet becomes evident form this figure.

applied in superposition to the field generated by the notch-coil magnet. The external perturbation field was generated by a simple solenoid coiled around the outer glass cylinder of the magnet system assembly. A ten turns solenoid (2 cm length and positioned with its center located around the geometric center of the magnet) powered by a current of $I = \pm 5$ A was used. This external field was treated like an arbitrary unknown source. Fig. 13 shows the results of these experiments ($V \approx 25$ cm^3), for the case of a perturbation

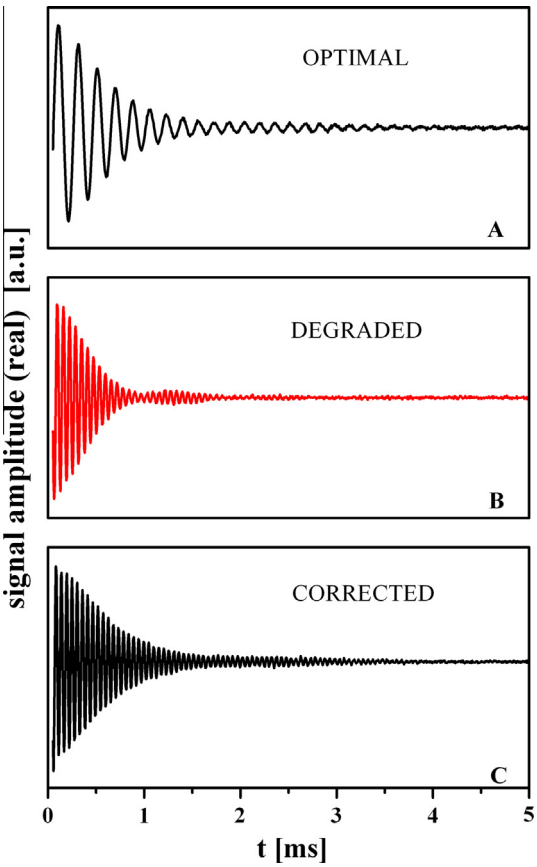

Fig. 13. Captured ^{1}H NMR signals showing the capacity of the magnet to compensate for homogeneity degradation produced by an external field. In A, the position of the notch layers was set to the optimal position and the current applied to the external solenoid was zero. In B, $d = d_{opt}$ and the current in the solenoid generating the degrading field was set to $I = 5$ A, adding a magnetic field against B_0. Figure C corresponds to the new position of the notch coils in the presence of the degrading field, with $d = d_{opt} - 0.375$ mm.

Table 3
Prediction of magnet performance for different materials.

Material	ρ (Ω m)	R (mΩ)	I (A)	U (V)	B (mT)
Al alloy	$5.20E-8$	174.9	239	41.8	150.5
Al pure	$2,65E-8$	89.3	335	29.9	210.5
Cu	$1.72E-8$	58.0	415	24.1	261.2
Ag	$1.59E-8$	53.5	432	23.1	271.9

field against the magnetic flux density generated by the magnet. In the figure, A corresponds to the unperturbed FID acquired at the optimal configuration. B shows the degraded FID after the application of the perturbation,while C show the compensated FID following the magnet reconfiguration. As it can be observed from the figure, the homogeneity degradation can be compensated by adjusting the position of the notch layers to a new position.

The switching performance of the notch-coil magnet was tested by monitoring the temporal evolution of the voltage at the shunt output available in the control-unit of the field-cycling apparatus. This shunt voltage, recorded with a Textronix TDS 2001 C (Beaverton, OR, USA) digital oscilloscope, is directly proportional to the current intensity I flowing through the magnet. Nevertheless, it is worth to mention that the switching performance not only depends on the electric properties of the magnet itself, but also on the power management network and control strategy used in the power supply. No energy storage assistance was used in this

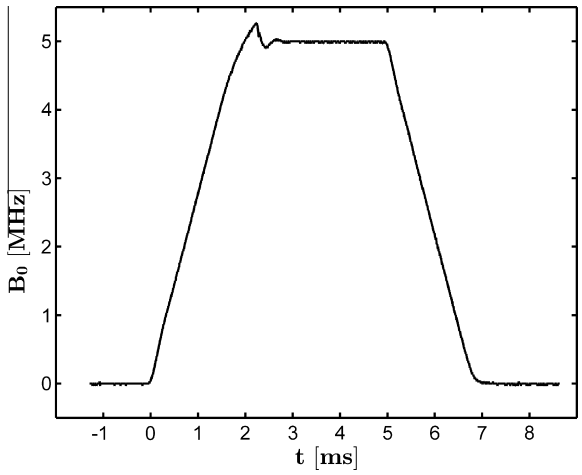

Fig. 14. Temporal evolution of the shunt voltage during a generated magnetic field pulse from zero to $B_0 = 5$ MHz.

test, just the electronic current regulation included in the Stelar's control unit. Fig. 14 shows the temporal evolution of the shunt voltage during a typical magnetic field pulse, from zero current in the magnet up to the corresponding to a magnetic field of $B = 5$ MHz. The AC-feedback of the control unit [2] was not optimized. This essentially means that the transient after switching may improve. The maximum slew rate s_R available under the current conditions is about $s_R = 2.54$ MHz ms^{-1} or $s_R = 59.6$ mT ms^{-1}.

5. Conclusions

We have shown that the notch-coil concept is suitable for field-cycling instruments. Even with only one inner cylinder, the resulting magnet performance is compatible with most low-resolution NMR experiments for sample volumes up to 35 cm^3. Since the design is based on a constant pitch helical structure, no complex computer-assisted machining tools are needed. The fact that the resulting homogeneity is slightly dependent on the precision of the cut favours this point. Only the cylinders diameters and lengths have to be machined with certain precision, still possible with a good quality standard lathe. A simple and efficient cutting tool was developed, thus turning the whole machining process cost-effective without the need of sophisticated mechanization tools. The purpose of using an aluminium alloy was mainly to simplify the machining process (copper is more difficult to mechanize) while avoiding an excessive cost during the first cutting trials (copper and silver are more expensive). Clearly the magnet performance would improve if a material having a lower resistivity is used. A prediction for different materials can be found in Table 3.

Using lower resistivity would improve the thermal response of the system and favour higher switching rates. However, the magnet homogeneity at low duty-cycle becomes practically independent on the material choice.

A PVC $\simeq 60\%$ for a 10 ppm homogeneity was used in the calculations. This means that 40% of the sample volume is subjected to a lower homogeneity. According to the field map depicted in Fig. 4, for a 35 cm^3 sample, the portion of the sample volume close to the sample container walls is subjected to a theoretical homogeneity ranging between 25 and 100 ppm. From the measured NMR signal corresponding to this volume we deduce an effective homogeneity of about 130 ppm. As usual in these comparatives, the experimental homogeneity is lower than the calculated, which we mainly attribute to mechanical imperfections of the magnet assembly. In our case, the influence of the incoming and outgoing

conductors on the field map was considered in the calculations. Thermal stress in the magnet may also contribute to the difference between calculated and measured homogeneity, although at low duty-cycle this effect may be of second order. The corresponding homogeneity measured for the 25 cm^3 sample is about 80 ppm.

From Fig. 3 we can see that a slightly more efficient magnet (in terms of field-to-power ratio) with more favourable electric characteristics is feasible, at the expense of a lower homogeneity. This choice has also a clear impact in the total machining time of the cylinders. In fact, a magnet having a lower N_{inner} would have a lower resistance and inductance values, thus offering better conditions for the switching performance. For example, for $N_{inner} = 80$, compared to $N_{inner} = 104$, the maximum field increases about 7%, the PVC is reduced about 20% and the resistance of the coil is reduced about 23%. Another decisive factor for the selection of the optimized configuration is the current intensity needed to reach the indicated maximum magnetic flux density B_{max} (10 kW). In fact, in the previous example, from 104 to 80 turns, the current increases about 39%. This also affects the thermal stress and cooling considerations. Thus "faster" coils with lower homogeneity are feasible and attractive for T_1-relaxometry applications at the expense of much higher current operation.

In contrast to variable pitch versions, the notch-coil has an uniformly distributed power dissipation and adjustable geometry. The uniform dissipation along the magnet body avoids localized heating. Therefore, the robustness of the magnet is much higher under extreme peak currents or operation at limiting conditions. At similar cooling conditions for equivalent magnets, the notch-coil version can operate at a higher regime. However, it is worth to note that under limiting conditions, the thermo-mechanical stress dramatically alters the magnet homogeneity (for both magnet types) while also shifting the mean value of the field. So far corrections have been implemented to correct the average field value, but not the homogeneity. The concept of variable geometry goes in this direction. A set of shimming coils may be considered as an efficient alternative to a variable geometry magnet. However, to be efficient, they have to be located between the inner wall of the magnet-system and the probe, thus reducing the available volume inside the magnet. In addition, if these coils are pulsed, they are not free of thermal effects and/or magnetic couplings with the magnet or other coils in the system (gradient coils, magnetic field compensation coils, etc.). An active magnet with improved homogeneity is desirable for MRI experiments, and probably, if requiring spectral resolution. A wide-bore design is useful not only for FFC-MRI, but also for T_1 relaxation dispersion experiments and 2D T_1 T_2 correlation spectra in large porous samples.

The stability of the magnet was preserved after proximately 500 h of operation (over a period of 6 moths).

Acknowledgments

We thank to Daniel Vicente and collaborators from the mechanical workshop for their assistance during this work. Economic support from Foncyt (Project PICT-2013-1380) is also acknowledged.

Appendix A

The homogeneity of the magnetic flux density in the central region of the variable notch-coil magnet was calculated by means of the Biot-Savart law. With the assumption that the helical current-carrying path is an infinite small wire, the z-component of the magnetic flux density at any spatial point $s_k = (x_k, y_k, z_k)$ for the inner layer can be computed from:

$$B_{z,inner}(x_k,y_k,z_k) = \frac{\mu_0 I}{4\pi}\left\{\int_{\varphi_1}^{\varphi_2} d\varphi \times \frac{-r\sin\varphi\cdot(y_k \pm r\sin\varphi) \pm r\cos\varphi\cdot(x_k - r\cos\varphi)}{[(x_k - r\cos\varphi)^2 + (y_k \pm r\sin\varphi)^2 + (z_k - p\cdot\varphi)^2]^{3/2}}\right\} \tag{2}$$

where r represents the mean radius of the cylinder, φ_1 and φ_2 the boundaries of the integral. They are defined for the inner layer as:

$$\begin{aligned}\varphi_1 &= -\frac{N_{inner}}{2}2\pi \\ \varphi_2 &= \frac{N_{inner}}{2}2\pi\end{aligned} \tag{3}$$

With this definition, the geometrical center of the magnet system is placed for the calculations at $x = 0, y = 0, z = 0$. The calculation of the z-components of the magnetic flux density for the two notch layers is similar to Eq. (2), but with positions and boundaries set to new values:

$$B_{z,notch}(x_k,y_k,z_k) = \frac{\mu_0 I}{4\pi}\left\{\int_{\varphi_1}^{\varphi_2} d\varphi \times \frac{-r\sin\varphi\cdot(y_k \pm r\sin\varphi) \pm r\cos\varphi\cdot(x_k - r\cos\varphi)}{[(x_k - r\cos\varphi)^2 + (y_k \pm r\sin\varphi)^2 + (z_k - p\cdot\varphi \pm d)^2]^{3/2}}\right\}. \tag{4}$$

The additional parameter d here is the same as l_{inner} and the corresponding boundaries for the notch layer are defined for the positive side as:

$$\begin{aligned}\varphi_{1pos} &= \frac{N_{inner}}{2}2\pi \\ \varphi_{2pos} &= \left(\frac{N_{inner}}{2} - N_{notch}\right)2\pi\end{aligned} \tag{5}$$

and for the negative side of the z-axis as:

$$\varphi_{1neg} = \left(-\frac{N_{inner}}{2} + N_{notch}\right)2\pi$$
$$\varphi_{2neg} = -\frac{N_{inner}}{2}2\pi \tag{6}$$

The field distribution inside the volume of interest is obtained after the superposition of these contributions (for more detail see [9]). The spatial homogeneity is calculated by comparing the flux density at different positions within the volume of interest, with the magnetic flux density at the center point $B(0,0,0)$:

$$\frac{\Delta B}{B} = \frac{B_z(0,0,0) - B_z(x_k,y_k,z_k)}{B_z(0,0,0)} \tag{7}$$

The calculus is performed within a cubic volume, which is divided into a cubic mesh. The coordinates (x_k,y_k,z_k) are located at each equidistant node of the mesh and the homogeneity estimation is expressed in parts per million (ppm). Eqs. (2) and (4) are numerically computed by means of an adaptive Gauss–Kronrod quadrature method [17,18] for each k-node of the mesh. Due to this numerical computation method and the assumption that the current-carrying path is approximated by a infinite small wire, the calculation of the magnetic flux density distribution requires low computational efforts as well as minor computational periods.

After the necessary parameters $(r_{i/inner}, r_{o/inner}, r_{i/notch}, r_{o/inner}, c, l_{inner})$ are defined, the missing parameters are encountered by the following procedure: for a certain number of turns of the inner layer (N_{inner}), the parameters N_{notch} and d are independently varied. Then, the combination of both parameters that yields the best spatial homogeneity is selected. In order to have an indication of the spatial homogeneity quality, a parameter called percentage volume coverage $(PVC_{homogeneity})$ is introduced.

$$PVC_{homogeneity} = \frac{N_{\leqslant homogeneity}}{N_{total}} \tag{8}$$

It represents the ratio of points which are below or equal to a predefined homogeneity value with respect to the total quantity of points k in percent.

References

[1] F. Noack, NMR field-cycling spectroscopy: principles and applications, Progr. Nucl. Magn. Reson. Spectrosc. 18 (1986) 171–276.
[2] E. Anoardo, G. Galli, G. Ferrante, Fast-field-cycling NMR: applications and instrumentation, Appl. Magn. Reson. 20 (2001) 365–404.
[3] R. Kimmich, E. Anoardo, Field-cycling NMR relaxometry, Progr. Nucl. Magn. Reson. Spectrosc. 44 (2004) 257–320.
[4] G. Ferrante, S. Sykora, Technical aspects of fast field cycling, Adv. Inorg. Chem. 57 (2005) 405–470.
[5] F. Fujara, D. Kruk, A. Privalov, Solid state field-cycling NMR relaxometry: instrumental improvements and new applications, Progr. Nucl. Magn. Reson. Spectrosc. 82 (2014) 39–69.
[6] C. Grossl, F. Winter, R. Kimmich, Optimisation of magnetic coils for NMR field-cycling experiments, J. Phys. E: Sci. Instrum. 18 (1985) 358–360.
[7] K.-H. Schweikert, R. Krieg, F. Noack, A high-field air-cored magnet coil design for fast-field-cycling NMR, J. Magn. Reson. 78 (1988) 77–96.
[8] O. Lips, A. Privalov, S. Dvinskikh, F. Fujara, Magnet design with high B_0 homogeneity for fast-field-cycling NMR applications, J. Magn. Reson. 149 (2001) 22–28.
[9] S. Kruber, G. Farrher, E. Anoardo, Comparative study of helical-cut notch-coil magnets for fast-field-cycling nuclear magnetic resonance, Can. J. Phys. 92 (2014) 1430–1440.
[10] H. Marshall, H. Weaver, Application of the Garrett method to calculation of coil geometries for generating homogeneous magnetic fields in superconducting solenoids, J. Appl. Phys. 34 (1963) 3175–3178.
[11] D. Kabat, L. Cesnak, J. Kokavec, Optimisation of inner-notch-corrected highly homogeneous superconducting solenoids and their comparison with other coil configurations, J. Phys. E: Sci. Instrum. 12 (1979) 652–657.
[12] R. Saunders, A. Zisserman, C.J. McCauley, The calculation of magnetostatic fields from axisymmetric conductors, J. Phys. D: Appl. Phys. 29 (1996) 533–539.
[13] R. Turner, Minimum inductance coils, J. Phys. E: Sci. Instrum. 21 (1988) 948–952.
[14] D. Yu, K. Han, Self-inductance of air-core circular coils with rectangular cross section, IEEE T. Magn. 23 (1987) 3916–3921.
[15] K.-B. Kim, E. Levi, Z. Zabar, L. Birenbaum, Mutual inductance of noncoaxial circular coils with constant current density, IEEE T. Magn. 33 (1997) 4303–4309.
[16] S. Babic, C. Akyel, Improvement in calculation of the self- and mutual inductance of thin-wall solenoids and disk coils, IEEE T. Magn. 36 (2000) 1970–1975.
[17] F. Cailó, W. Gautschi, E. Marchetti, On the computing gauss-kronrod quadrature formulae, Math. Comput. 47 (1986) 639–650.
[18] L. Shampine, Vectorized adaptive quadrature in matlab, J. Comput. Appl. Math. 211 (2008) 131–140.